Mineralogical Magazine, April 2016, Vol. 80(2), pp. 325–335

$Cu_{0.8}Mg_{1.2}Si_2O_6$: a copper-bearing silicate with the low-clinopyroxene structure

Lei Ding, Céline Darie, Claire V. Colin and Pierre Bordet*

Université Grenoble Alpes, Institut Néel, Grenoble, 38042, France CNRS, Institut Néel, Grenoble, 38042, France

[*Received 18 January 2015; Accepted 20 May 2015; Associate Editor: David Hibbs*]

ABSTRACT

The $Cu_{0.8}Mg_{1.2}Si_2O_6$ pyroxene has been synthesized using a soft chemistry method. Its crystal structure was determined from powder X-ray diffraction data. $Cu_{0.8}Mg_{1.2}Si_2O_6$ crystallizes with the low-clinopyroxene monoclinic structure (space group $P2_1/c$). The role of the Jahn-Teller-distorted Cu^{2+} cation on the stability of this strongly distorted structure is investigated. Cu^{2+} shows a strong preference for the M2 site, attributed to a better adaptation of its JT-distorted coordination polyhedron to this already distorted and more flexible site. Comparison with previously reported compounds indicates that increasing the Cu content enhances the M2 site distortion, eventually leading to symmetry lowering from orthorhombic *Pbca* to monoclinic $P2_1/c$. These observations bring new insight into the mechanisms of formation and chemical composition of pyroxene minerals in the presence of JT cations.

Keywords: pyroxene, crystal structure, Jahn-Teller effect.

Introduction

Compounds of the pyroxene family form one of the most abundant mineral species in the Earth's crust and upper mantle, and have therefore been subject to a wealth of detailed studies investigating their structures and crystallo-chemistry, depending on composition, formation conditions, and so on. Pyroxene compounds with the chemical formulas $M2M1Si_2O_6$ (M1 = di- or trivalent transition metals, M2 = mono- or divalent metals) are generally found in three main forms, orthopyroxene, high clinopyroxene and low clinopyroxene, with space groups *Pbca*, $C2/c$ and $P2_1/c$, respectively. Their structures are built up by chains of edge-sharing M1 and M2 octahedra aligned along the c axis, linked by chains of SiO_4 tetrahedra, and considerable effort has been given to understand the relation between the pyroxene composition and its structural topology (Cameron and Papike, 1981; Redhammer and Roth, 2004; Thompson and Downs, 2003, 2004; Thompson *et al.*, 2005). In this regard, pyroxenes containing Jahn-Teller (JT) cations have been subject to particular attention. Difficulty in accommodating the corresponding polyhedral distortions may play a role in the ability of pyroxenes to contain large amounts of JT cations.

Recently, pyroxenes containing magnetic cations have attracted new interest from a different viewpoint because some of them were found to present multiferroic properties (Jodlauk *et al.*, 2007; Kim *et al.*, 2012; Redhammer *et al.*, 2011, 2013), magnetoelectric effects (Nenert *et al.*, 2010*a*,*b*; Redhammer *et al.*, 2009), and quasi-one-dimensional (Q1D) magnetic behaviour (Valenti *et al.*, 2002). These physical properties are due to their unique crystal structure. Competition between inter- and intra-chain magnetic interactions leads to magnetic frustration and the appearance of various exotic magnetic properties such as a spin singlet ground state (Sasago *et al.*, 1995) and spin-Peierls transitions (Isobe *et al.*, 2002). In this respect, copper-containing pyroxenes are of foremost interest due to the spin ½ of Cu^{2+} cations, which could lead to enhanced quantum effects.

According to previous investigations, the magnetic configuration in pyroxene compounds can be

*E-mail: pierre.bordet@neel.cnrs.fr
DOI: 10.1180/minmag.2016.080.002

changed via chemical substitution at the M1 and/or M2 sites. In the case of $CaCuGe_2O_6$ the behaviour of magnetization was interpreted as due to a spin-singlet ground state (Sasago *et al.*, 1995). *Ab initio* calculations indicated that this behaviour derives from intra-chain interactions of Cu^{2+} dimers (Valenti *et al.*, 2002). Later on, Redhammer *et al.* (2005) showed that $CaCuGe_2O_6$ has the clino-pyroxene structure, space group $P2_1/c$, at room temperature. As magnetic properties are influenced strongly by interatomic distances in this family of materials, it is tempting to look for compounds where Ge cations are substituted by smaller Si cations. To our knowledge, $CaCuSi_2O_6$ preparation was never reported and, despite many attempts, we were unable to synthesize it. For the larger Ba cation, $BaCuSi_2O_6$ adopts the Han purple crystal structure (Finger *et al.*, 1989; Sparta and Roth, 2004). Attempts to synthesize $MgCuSi_2O_6$ by soft chemistry methods lead to the preparation of a compound with a composition close to $CuMgSi_2O_6$. The existence of the $CuMgSi_2O_6$ pyroxene was reported by Breuer *et al.* (1986), but only the cell parameters and a tentative space group were given. In fact, the only other Cu-bearing pyroxene silicate for which a complete structure analysis was reported is the orthopyroxene $(Cu_{0.44}Mg_{1.56})Si_2O_6$ (Tachi *et al.*, 1997), space group *Pbca*. It is important to note that, at variance with $CaCuGe_2O_6$, here the Cu^{2+} cations occupies the M2 site; this may have a considerable impact on physical properties. Here we report the synthesis based on the preparation of a precursor by a soft chemistry method and detailed structural analysis of $Cu_{0.8}Mg_{1.2}Si_2O_6$, which can bring valuable insight into the role of the Jahn-Teller effects in metal site selectivity, structure distortion and chemical composition in pyroxene compounds.

Experimental

Sample preparation and characterization

For a typical synthesis of 1 g of $CuMgSi_2O_6$ the stoechiometric quantities of $Cu(C_2H_3O_2)_2.H_2O$, $Mg(C_2H_3O_2)_2.4H_2O$, and tetraethoxysilane (TEOS: $C_8H_{20}O_4Si$, 99.9%) were dissolved in 50 ml ethanol with vigorous stirring at 110°C for 3 h. The solution was dried at 60°C for several hours in order to remove solvents before further thermal treatment. The resulting precursor was calcined between 800°C and 1000°C (between 10 and 50 h, with intermediate regrinding) in air. This temperature range was chosen in order to avoid reduction of Cu^{2+} to Cu^{1+}, known to occur at ~1020°C in air.

A thermogravimetrical (TG and DSC) analysis was carried out using a Netzsch Thermal Analysis System to investigate the behaviour of the precursor with varying temperature. TG-DSC curves were recorded for ~20.9 mg of precursor powder placed in an alumina crucible, by warming and cooling at a rate of 10°C min^{-1} between RT and 800°C. A mixed atmosphere (Ar 80% and O_2 20%) was used.

Morphology and chemical composition were investigated by field-emission scanning electron microscopy (FESEM, Zeiss Ultraplus) equipped with an energy-dispersive X-ray spectrometer (EDX, Bruker). The sample was gold-coated prior to SEM and EDX analysis.

The zero field cooling (ZFC) and field cooling (FC) temperature dependence of magnetic susceptibility for $Cu_{0.8}Mg_{1.2}Si_2O_6$ was measured between 5 and 350 K on a Quantum Design, MPMS-XL SQUID magnetometer.

Powder X-ray diffraction

All samples were characterized using powder X-ray diffraction (XRD) data collected with a Siemens D5000 diffractometer in transmission geometry, using a focusing Ge(111) monochromator for Cu$K\alpha_1$ radiation and a linear PSD. For structure solution and refinement, a diffraction pattern was collected on the best sample obtained in terms of purity and crystallinity (sample n°6 in Table 1). Measurements were carried out at room temperature in the 10–90°2θ range with a step size of 0.032°. The *Fox* program (Favre-Nicolin and Cerny, 2002), was used to index the pattern, determine the most probable space group and provide a starting model for structure refinement, which was carried out by the Rietveld method using the *Fullprof* program (Rodríguez-Carvajal, 1993). Background was described by linear interpolation of selected points in the pattern. A Thomson-Cox-Hastings model (Thompson *et al.*, 1987) of the reflection profile including anisotropic peak broadening was used. The size broadening effect was described using a uniaxial model with *b* as the unique axis, while a tensor description was applied for strain. Low-angle peak asymmetry was taken into account using the Bérar-Baldinozzi model (Bérar and Baldinozzi, 1993). In order to reduce the number of structural parameters, atoms of the same element were given equal isotropic displacement parameters. For the two metal sites, the composition was refined assuming

https://doi.org/10.1180/minmag.2016.080.002 Published online by Cambridge University Press

TABLE 1. Summary of synthesis conditions and resulting sample composition and pyroxene phase stoichiometry for $CuMgSi_2O_6$.

No.	Starting materials	Calcination condition	Results and phases (wt.%)			Composition	
			Sample comp.	SiO_2	CuO	Cu	Mg
1	Cu acetate, Mg acetate, TEOS	1000°C, 10 h	95.09(1.95)	1.48(0.19)	3.44(0.13)	0.79(2)	1.21(2)
2	Cu acetate, Mg acetate, TEOS	1000°C, 40 h	93.91(1.47)	1.84(0.20)	4.25(0.15)	0.80(2)	1.20(2)
3	Cu acetate, Mg acetate (>3 mol.%), TEOS	1000°C, 10 h	91.10(1.35)	1.12(0.19)	7.78(0.15)	0.79(2)	1.21(2)
4	Cu acetate, Mg acetate (>6 mol.%), TEOS	1000°C, 10 h	93.86(0.73)	4.11(0.07)	2.04(0.05)	0.81(1)	1.19(1)
5	Cu acetate, Mg acetate (>6 mol.%), TEOS	1000°C, 50 h, regrinding	95.94(0.61)	3.72(0.08)	0.34(0.04)	0.81(1)	1.19(1)
6	Cu acetate, Mg acetate (>6 mol.%), TEOS	1000°C, 10 h	98.89(0.06)	<0.5 (excluded)	1.11(0.06)	0.79(1)	1.21(1)
7	Cu acetate, Mg acetate (>10 mol.%), TEOS	1000°C, 10 h	94.81(1.41)	2.91(0.21)	2.28(0.12)	0.86(2)	1.14(2)
8	Cu acetate, Mg acetate (>20 mol.%), TEOS	1000°C, 10 h	79.81(1.00)	9.06(0.36)	11.12(0.14)	0.77(1)	1.23(1)

possible substitution between Cu and Mg with full total site occupancies. The global Cu/Mg stoichiometry was left unconstrained. A small amount of CuO and probably SiO_2 were detected as impurities; only CuO was introduced in the pattern description and its cell parameters and scale factor were refined. The final refinement yielded a weight fraction of 1.11(6)% for this phase. A single weak reflection tentatively attributed to SiO_2 at 21.9°2θ was excluded from the pattern.

Results and discussion

Synthesis and characterization

Pyroxene compounds are prepared classically using solid-state reaction techniques at elevated temperatures, and sometimes high-pressure conditions. Single crystals may also be obtained using flux growth methods, as for example reported by Tachi *et al.* (1997) for Cu-bearing orthopyroxene $Cu_{0.44}Mg_{1.56}Si_2O_6$. In this case, the amount of copper introduced in the pyroxene framework was rather limited. In our work, many efforts to synthesize the $CuMgSi_2O_6$ compound have been made via a traditional solid-state reaction with intermediate grinding according to Breuer *et al.* (1986), but they systematically resulted in mixtures of CuO, MgO, SiO_2, Mg_2SiO_4 and other clinopyroxene phases. The amount of impurity phases precluded an accurate physical and structural analysis of the samples. Therefore, we decided to investigate a soft chemistry route for the preparation of a precursor. The best results were obtained with the method described above. Typical yields depending on preparation conditions are summarized in Table 1. All the samples were submitted to Rietveld refinement of powder XRD data to determine the proportion of impurity phases as well as the pyroxene phase stoichiometry. The samples obtained contained the clinopyroxene compound as the major phase, plus impurities (SiO_2, CuO), depending mainly on the starting composition of the solution. It is worth noting that the amounts of impurity phases are systematically much less than in the case of a standard solid-state reaction. In order to obtain an almost single phase clinopyroxene sample, it was necessary to use a 6 mol.% excess magnesium acetate. An annealing time of 10 h at 1000°C was generally used. Longer annealing times, including intermediate regrinding, led to a small decrease of the proportion of impurity phases but did not modify the pyroxene phase Cu/Mg content (compare for example, samples 4 and 5). In fact, this composition was essentially independent of synthesis conditions. Moreover, no significant improvement in sample crystallinity as seen from Bragg peak widths and shapes could be detected for longer annealing times. This seems to indicate that a stoichiometric $CuMgSi_2O_6$ compound cannot be prepared under these synthesis conditions. Sample 6 in Table 1 was selected for the detailed structural analysis reported below.

https://doi.org/10.1180/minmag.2016.080.002 Published online by Cambridge University Press

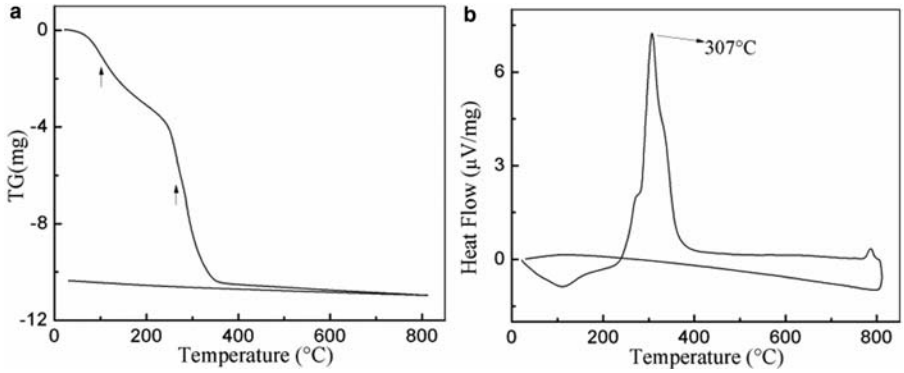

FIG 1. TG-DSC curves for the $CuMgSi_2O_6$ precursor.

As shown in Fig. 1*b*, a weak endothermic peak is observed in the DSC curve around 100°C which probably corresponds to the evaporation of water and other remaining solvents. A corresponding small mass decrease upon heating is also detected in the TG curve at a similar temperature (Fig. 1*a*). Moreover, a strong exothermic peak observed at 307°C in the DSC curve can be attributed to the decomposition of organic species from the precursor. This is confirmed by the strong decrease of mass in the TG curve observed at the same temperature. No marked mass change is then observed up to 800°C, indicating full decomposition of these species. A small exothermic peak is observed on the DSC curve just below 800°C. As no other feature is observed, it can be attributed to the formation reaction of the pyroxene.

The SEM observations show that the sample is composed of crystalline grains with a roughly cylindrical shape with a diameter up to ~1 μm, as shown in Fig. 2. Prominent circular stripes are observed on the surface of each grain at higher magnification, suggesting that the cylinder axis is the preferred growth direction. The Cu/Mg ratio obtained using EDX by averaging the compositions from 12 different points was 0.8(1).

Structural study

Refinement results, main interatomic distances and bond-valence sums calculated using the *BonStr* program (Rodríguez-Carvajal, 2010) are presented in Tables 2 and 3. The final Rietveld refinement plot is shown in Fig. 3. Some information about the structure of $CuMgSi_2O_6$ has been reported previously by Breuer *et al.* (1986), although a full structural analysis was not performed. The authors proposed that $CuMgSi_2O_6$ crystallizes with monoclinic $P2_1/c$ symmetry and unit-cell parameters a = 9.731, b = 8.918, c = 5.224 Å, β = 110.52°. The results of our *ab initio* structure determination and

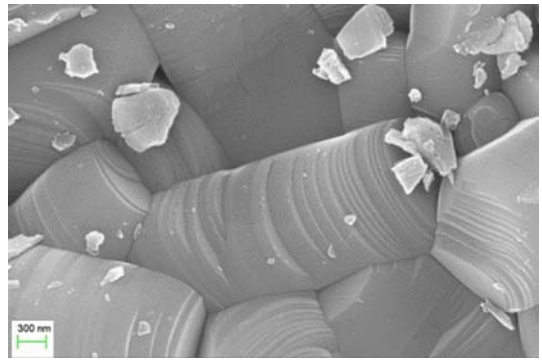

FIG 2. SEM image for the $Cu_{0.8}Mg_{1.2}Si_2O_6$ compound.

https://doi.org/10.1180/minmag.2016.080.002 Published online by Cambridge University Press

TABLE 2. Agreement factors and refined structural parameters for $Cu_{0.8}Mg_{1.2}Si_2O_6$.*

Name	pos.	*x/a*	*y/b*	*z/c*	*B* (Å^2)	occupancy
SiA	4*e*	0.0496(7)	0.3388(8)	0.2926(11)	1.63(8)	1.0
SiB	4*e*	0.5497(7)	0.8368(8)	0.2571(11)	1.63(8)	1.0
M1 Mg/Cu	4*e*	0.2504(10)	0.6506(5)	0.2266(14)	0.95(14)	0.930/0.070 (7)
M2 Cu/Mg	4*e*	0.2545(5)	0.0054(2)	0.2286(7)	1.26(8)	0.72/0.28 (1)
O1A	4*e*	0.8768(14)	0.3376(14)	0.176(2)	0.95(10)	1.0
O2A	4*e*	0.1256(11)	0.5040(12)	0.3416(18)	0.95(10)	1.0
O3A	4*e*	0.1062(10)	0.2740(9)	0.617(2)	0.95(10)	1.0
O1B	4*e*	0.3683(13)	0.8385(14)	0.1353(18)	0.95(10)	1.0
O2B	4*e*	0.6422(12)	0.9825(12)	0.4087(18)	0.95(10)	1.0
O3B	4*e*	0.6019(10)	0.7033(10)	0.496(2)	0.95(10)	1.0

*Space Group: $P2_1/c$; $a = 9.7352(1)$, $b = 8.90197(8)$, $c = 5.22676(6)$ Å, $\beta = 110.721(1)°$, $R_p = 2.92$, $R_{wp} = 4.07$, $R_{exp} = 1.60$, $\chi^2 = 6.46$, $R_{Bragg} = 3.02$.

Rietveld refinement are in good agreement with the unit cell and symmetry proposed previously, with $a = 9.7352(1)$, $b = 8.90198(8)$, $c = 5.22676(6)$ Å and $\beta = 110.721(1)°$, $V = 423.662(7)$ Å^3, with space group $P2_1/c$.

The structure is shown in Fig. 4. This compound belongs to the well-known family of low clinopyroxenes with space group $P2_1/c$ for which all atoms are located in 4*e* general positions. This structure is characterized by alternate stacking perpendicular to the *a* axis of layers made of SiO_4 tetrahedra and layers made of MO_6 octahedra (M = Cu, Mg). Each tetrahedron in a layer shares two corners with two adjacent tetrahedra to form zigzag chains running along the *c* axis direction (Fig. 5). The bases of the tetrahedra are roughly parallel to the (100) plane and all tetrahedra in a given chain point in the same direction along the *a* axis. Two consecutive chains along the *b* axis have their tetrahedra pointing in opposite directions. All Si cations in a given layer are equivalent by symmetry; SiA and SiB layers alternate along the *a* axis. The SiA tetrahedra are more distorted with a smaller average Si–O bond length of 1.62(1) Å (bond-valence sum, BVS = 4.10(7)), while SiB tetrahedra are more regular with a larger average bond length of 1.65(1) Å, resulting in slight underbonding (BVS = 3.75(6)). It is also worth noting that the degrees of extension of the tetrahedral chains, as characterized by the angle between three consecutive tetrahedra-linking oxygen anions along a chain, are quite different for SiA (O3A–O3A–O3A = 161.4(5)°) and SiB chains (O3B–O3B–O3B = 144.7(5)°).

TABLE 3. Principal cation-anion distances (Å) for $Cu_{0.8}Mg_{1.2}Si_2O_6$.

SiA–O1A	1.57(1)	SiB–O1B	1.65(1)
–O2A	1.63(1)	–O3B	1.67(1)
–O3A	1.69(1)	–O3B	1.65(1)
–O3A	1.58(1)	–O2B	1.62(1)
Ave. Dist.	1.62	Ave. Dist.	1.65
BVS	4.10(7)	BVS	3.75(6)
M1–O1A	2.24(1)	M2–O1A	2.14(1)
–O1A	2.03(1)	–O2A	1.963(9)
–O2A	2.01(1)	–O3A	2.384(9)
–O1B	2.17(1)	–O1B	2.01(1)
–O1B	2.04(1)	–O2B	1.808(9)
–O2B	2.09(1)	–O3B	2.76(1)
Ave. Dist.	2.10	Ave. Dist.	2.18
BVS	Mg^{2+}: 2.06(3)/ Cu^{2+}: 1.98(3)	BVS	Cu^{2+}: 2.06(3)/ Mg^{2+}: 2.14(3)

BVS = bond-valence sum.

In the octahedral layer (Fig. 6), the so-called pyroxene M1 sites are almost entirely (93.0(7)%) occupied by Mg^{2+} cations. The $M1O_6$ octahedra share their O1A–O1B edges to form zigzag chains along the *c* axis. They are only moderately distorted with distances ranging from 2.01(1) to 2.24(1) Å and an average bond length of 2.10(1) Å, in good agreement with the Mg^{2+} ionic radius (0.72 Å; Angel *et al.*, 1989). This distance is close to that reported for enstatite, $MgSiO_3$ (2.084(2) Å). The pyroxene M2 site is occupied mainly by Cu^{2+} cations (72(1)%) but also by Mg^{2+} cations

https://doi.org/10.1180/minmag.2016.080.002 Published online by Cambridge University Press

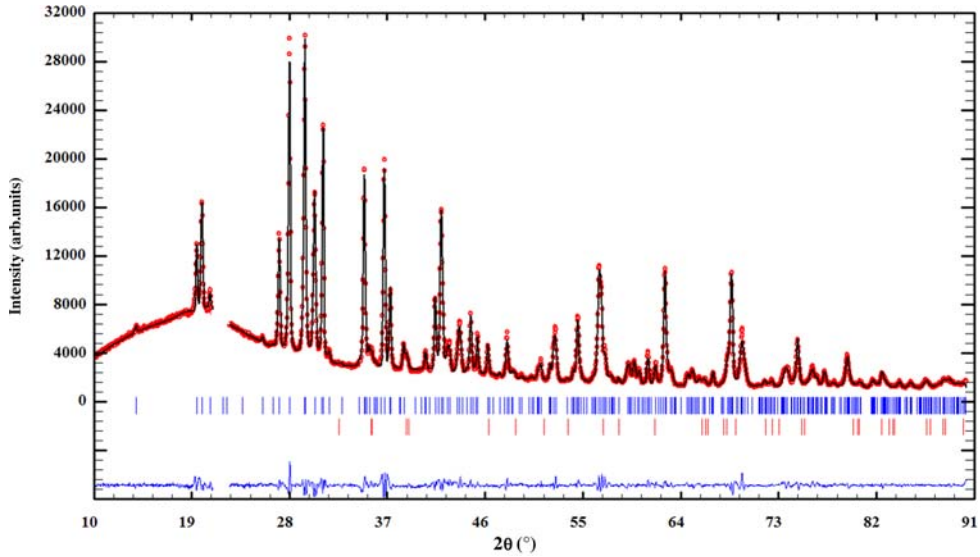

FIG 3. Rietveld plot for the refinement of $Cu_{0.8}Mg_{1.2}Si_2O_6$ from PXRD data. Tick marks denote Bragg reflections. The lower set of tick marks belongs to a CuO impurity phase.

(28(1)%). The overall stoichiometry as found by powder XRD is then $Cu_{0.8}Mg_{1.2}Si_2O_6$ and the Cu/Mg stoichiometric ratio (0.65) is reasonably close to that found by EDX. Each M2 cation octahedron is connected by edge sharing to three consecutive M1 cation octahedra along one M1 zigzag chain. The M2 octahedra are not connected to each other, and the shortest M2–M2 distances are 5.245(4) Å across an M1 chain, 5.227(6) Å on the same side of an M1 chain and 5.079(4) Å for two M2 octahedra attached to two neighbouring M1 chains. In contrast to the M1 site, the M2 octahedral site is strongly distorted with M2–O distances ranging between 1.808(9) and 2.76(1) Å. The four shorter bonds (1.808(9) to 2.14(1) Å) correspond to the O1A, O2A, O1B, and O2B anions shared with M1 octahedra. The remaining O3A and O3B anions are shared between the M2 octahedra and the Si tetrahedra of the chains above (O3A to SiA, M2A–O3A = 2.384(9) Å) and below (O3B to SiB, M2A–O3B = 2.76(1) Å) the octahedra layers. This latter M2A–O3B distance corresponds only to

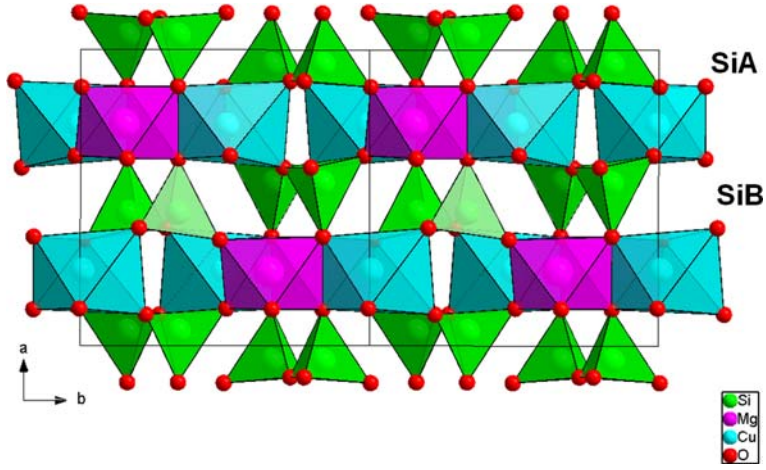

FIG 4. Projection of the $Cu_{0.8}Mg_{1.2}Si_2O_6$ structure along the *c* axis.

https://doi.org/10.1180/minmag.2016.080.002 Published online by Cambridge University Press

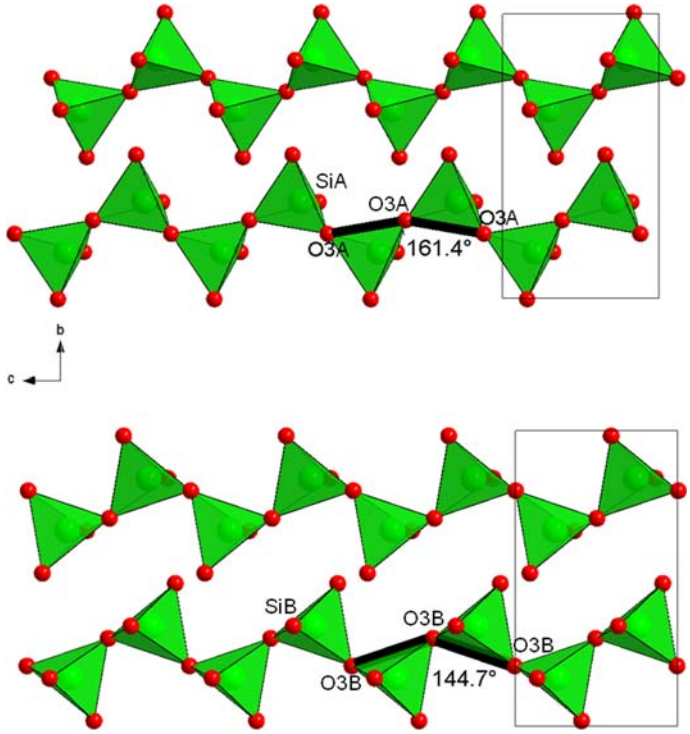

FIG 5. Projection of the SiA (top) and SiB (bottom) tetrahedra layers along the *a* axis.

negligible bond strength of 0.06 valence units (vu) and therefore the M2 cation can be considered as coordinated rather by a distorted square pyramid than by an octahedron of oxygen anions. Both tetrahedral chains connect the M2 octahedra of two consecutive M1–M2 octahedral chains. The SiA tetrahedra share one O2A–O3A edge with the M2 octahedra, while all other connections are made via corner sharing. SiB tetrahedra are only connected by corner sharing, resulting in a less distorted geometry.

Magnetic Properties

As shown in Fig. 7, the compound exhibits paramagnetic behaviour in the entire measured temperature range. No difference can be observed between the field-cooled and zero-field-cooled magnetization curves. The solid line in Fig. 7 represents the Curie fit using $\chi(T) = C/T + \chi_0$ in the temperature range 15–350 K, where C is the Curie constant and χ_0 a diamagnetic contribution. The fit yields $C = 0.413(2)$ and $\chi_0 = 2(3) \times 10^{-5}$ emu mol^{-1}, giving an effective moment $\mu_{eff} = 1.82\ \mu_B/Cu^{2+}$ which is very close to the expected spin-only value, 1.73 μ_B. This is in strong contrast with the magnetic behaviour observed for $CaCuGe_2O_6$, for which antiferromagnetic interactions and a spin-singlet ground state with a finite energy gap have been reported (Sasago *et al*., 1995; Redhammer *et al*., 2005). However, in the latter case, the Cu^{2+} cations occupy the M1 site of the pyroxene structure and interact strongly with first neighbour Cu–Cu distances of 3.072 Å (Redhammer *et al*., (2005), to be compared to distances above 5 Å for Cu^{2+} cations on the M2 site for $Cu_{0.8}Mg_{1.2}Si_2O_6$. The absence of magnetic ordering observed for $Cu_{0.8}Mg_{1.2}Si_2O_6$ is thus related directly to the weakness of magnetic interactions due to the structural arrangement.

Discussion

Although the pyroxene structure is known to accommodate a vast diversity of cations, copper-bearing pyroxenes are quite rare. Indeed, $CaCuGe_2O_6$ is the only known stoichiometric compound with the pyroxene structure (Breuer

https://doi.org/10.1180/minmag.2016.080.002 Published online by Cambridge University Press

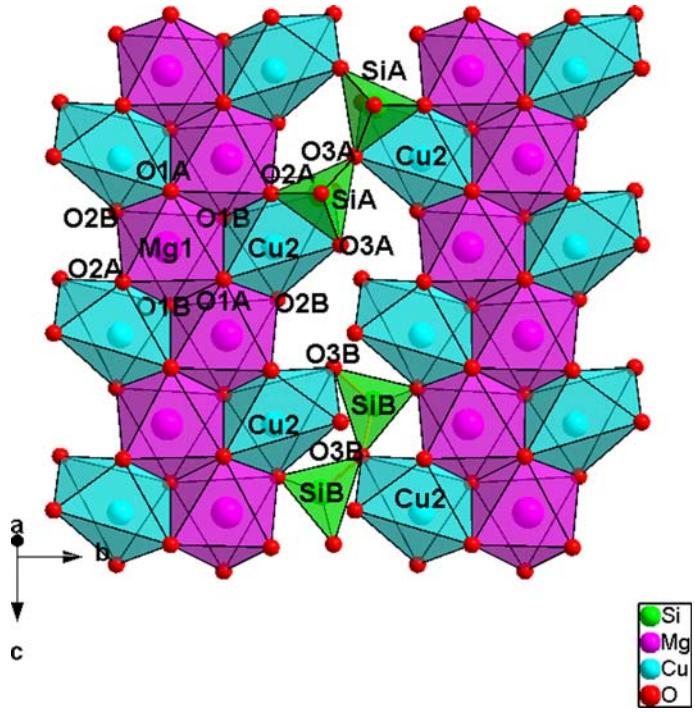

FIG 6. Structural arrangement of the M1, M2 octahedra layer of $Cu_{0.8}Mg_{1.2}Si_2O_6$. Some of the linking $SiAO_4$ and $SiBO_4$ tetrahedra are also represented.

et al., 1986; Redhammer *et al.*, 2005). Breuer *et al.* (1986) also reported a study of the $(MgMg)Si_2O_6$ – $(CuCu)Si_2O_6$ system with a solid solution limit attributed to $CuMgSi_2O_6$. However, only cell parameters and a tentative $P2_1/c$ space group were provided. Later on, the preparation and structural study of $Cu_{0.44}Mg_{1.56}Si_2O_6$ with the orthopyroxene structure (space group *Pbca*) were described (Tachi *et al.*, 1997). Here we report a study of the low-clinopyroxene compound (space group $P2_1/c$) with chemical composition $Cu_{0.8}Mg_{1.2}Si_2O_6$. It is worth noting that the samples obtained by Breuer *et al.* were prepared by reaction in air at 1000°C of an oxide mixture over very long reaction times (up to several weeks) and the orthopyroxene compound was obtained as a flux-grown single crystal at 850°C. Here, *quasi* single-phase powder samples were obtained through the preparation of a precursor by a soft chemistry route followed by a 10 h calcination step at 1000°C. This process appears to be very effective for the preparation of pyroxene-type oxides.

As Mg^{2+} and Cu^{2+} have almost the same ionic radius, the scarcity of Cu-bearing pyroxenes and the difficulty of substituting Mg for Cu in enstatite cannot be attributed only to steric effects. The JT distortion of Cu^{2+} coordination polyhedra has to be invoked. The present compound therefore provides a unique opportunity to better understand the role of the JT effect in the crystallo-chemistry of pyroxenes by comparison with the structures of Cu-bearing orthopyroxene (Cu-OP; (Tachi *et al.*, 1997) and enstatites where Mg is partly replaced by other JT cations such as Cr^{2+} (Cr-CP; Angel *et al.*, 1989). As enstatite is one of the most abundant minerals in the Earth's crust and upper mantle, a useful comparison is of interest for geochemists to understand the mineral formation and composition from Earth magma in the presence of JT cations.

A first and striking observation is the marked preference of JT cations for the M2 site in the case of pyroxene-type silicates. In the present work (Cu-CP), 7% of the M1 site was occupied by Cu^{2+}, 5.4% by Cr^{2+} in Cr-CP and full Mg occupancy was reported in Cu-OP. This strong site selectivity is very probably related to the topology of the pyroxene structure. The configuration of the M1 chains formed by edge-sharing octahedra is unfavourable for strongly distorted polyhedra. This well-known effect is observed in

https://doi.org/10.1180/minmag.2016.080.002 Published online by Cambridge University Press

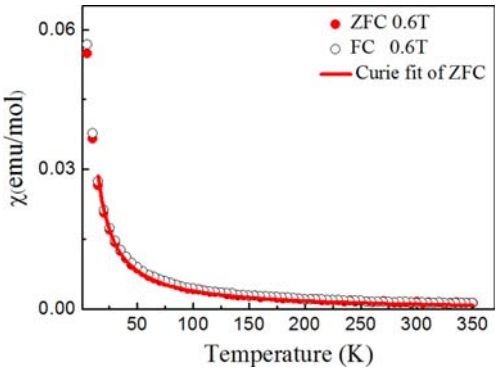

FIG 7. Temperature dependence of ZFC and FC magnetic susceptibility for $Cu_{0.8}Mg_{1.2}Si_2O_6$ under a 0.6 T magnetic field. The solid line represents the Curie-type fit to the data between 15 and 350 K.

pyroxene without JT cations such as enstatite for which the M2 site is markedly distorted with Mg–O distances ranging between 1.985(1) to 2.414(1) Å compared to 2.006(2) to 2.179(1) Å for the M1 site (Ohashi and Finger, 1976). In this case the distortion is a consequence of the steric mismatch between the octahedral and tetrahedral chains which constitute the structure. This pre-existing distortion is very probably a major cause for the site preference of JT cations for the M2 site. Moreover, as pointed out by Tachi *et al.* (1997), the presence of JT cations leads to an increase of the M2 site distortion. In order to quantify this effect, polyhedral distortion calculated by using the volume distortion parameter v (%) proposed by Makovicky and Balic-Zunic (1998) and computed using the *BondStr* program are reported in Table 4 for the M2 site polyhedra of Cu-OP, Cu-CP, and Cr-CP and clinoenstatite (Mg-CP) (Ohashi and Finger, 1976), together with the M2–O bond lengths and their relative changes with respect to the Mg-CP average M2–O bond length. Both Cu-bearing pyroxenes show very similar average M2–O bond lengths, somewhat larger than that of Mg-CP which may be due to the slightly larger ionic radius of Cu^{2+} (0.73 Å) *vs.* Mg^{2+} (0.72 Å). The distortion scheme of Mg-CP is clearly respected in Cu-OP and Cu-CP, in that the same bonds are elongated or shortened with respect to the average M2–O bond length in Mg-CP. The gradual replacement of Mg^{2+} by Cu^{2+} leads to a strong increase of the distortion while keeping the same scheme; short bonds become shorter and long bonds become longer. Moreover, the M2–O3A, –O2B and –O3B bonds which differ the most from the average are those which undergo the largest changes (from 2.279(1) to 2.384(9) Å for M2–O3A, 1.985(1) to 1.808(9) Å for M2–O2B and 2.414(1) to 2.76(1) Å for M2–O3B). Depending on the bonds, this effect may be quite non-linear with respect to the Cu content of the M2 site. For example, the longest distance, M2–O3B, changes very strongly from Mg-CP to Cu-OP, but only little from Cu-OP to Cu-CP (2.414(1) to 2.732(2) to 2.76(1) Å with a Cu content of 0 to 0.44 to 0.80, respectively). The first change indicates that O3B has to be considered as part of the M2 coordination for small Cu contents, as it is highly sensitive to the M2-site composition change. However,

TABLE 4. Comparison of M2–O distances (Å) for clinoenstatite ($Mg_{1.56}Cu_{0.44}Si_2O_6$), orthopyroxene ($Mg_{1.2}Cu_{0.8}Si_2O_6$, this work) and $Mg_{1.425}Cr_{0.611}Si_{1.946}O_6$. The relative change (%) with respect to the enstatite average bond length is shown in the second column. The average distance, polyhedral distortion and bond-valence sums are also given.

$MgSiO_3$ $P2_1/c$ (Ohashi *et al.*, 1976)			$Mg_{1.56}Cu_{0.44}Si_2O_6$ *Pbca (Cu–OP)* (Tachi *et al.*, 1997)			$Mg_{1.2}Cu_{0.8}Si_2O_6$ $P2_1/c$ *(Cu–CP)* (this work)			$Mg_{1.425}Cr_{0.611}Si_{1.946}O_6$ $P2_1/c$ *(Cr–CP)* (Angel *et al.*, 1989)		
at1–at2	dist.	Change	at1–at2	dist.	Change	at1–at2	dist.	Change	at1–at2	dist.	Change
Mg2–O1A	2.090(1)	–2.43	Cu2–O1A	2.115(2)	–1.26	Cu2–O1A	2.14(1)	–0.09	Cr2–O1A	2.180(7)	1.77
Mg2–O2A	2.032(1)	–5.14	Cu2–O2A	1.970(2)	–8.03	Cu2–O2A	1.969(9)	–8.08	Cr2–O2A	2.035(5)	–5.00
Mg2–O3A	2.279(1)	6.40	Cu2–O3A	2.340(2)	9.24	Cu2–O3A	2.384(9)	11.30	Cr2–O3A	2.281(5)	6.49
Mg2–O1B	2.053(1)	–4.15	Cu2–O1B	2.048(2)	–4.39	Cu2–O1B	2.01(1)	–6.16	Cr2–O1B	2.092(6)	–2.33
Mg2–O2B	1.985(1)	–7.33	Cu2–O2B	1.934(2)	–9.71	Cu2–O2B	1.808(9)	–15.59	Cr2–O2B	2.008(5)	–6.26
Mg2–O3B	2.414(1)	12.70	Cu2–O3B	2.732(2)	27.54	Cu2–O3B	2.76(1)	28.85	Cr2–O3B	2.648(5)	23.62
Average distance: 2.1420(6)			Average distance: 2.190(1)			Average distance: 2.178(5)			Average distance: 2.207(2)		
Distortion: 50.815×10^{-4}			Distortion: 158.283×10^{-4}			Distortion: 206.013×10^{-4}			Distortion: 96.873×10^{-4}		
Valence Sum: 1.922(3)			Valence Sum: 1.859(5)			Valence Sum: 2.06(3)			Valence Sum: 2.00(1)		

https://doi.org/10.1180/minmag.2016.080.002 Published online by Cambridge University Press

for larger Cu contents, the M2–O3B bond valence is only ~0.05 vu so that O3B can hardly be considered as part of M2 coordination, as stated above. In that sense, the M2 coordination polyhedron of both Cu-bearing pyroxenes can rather be described as a distorted square pyramid and the O3B ion is probably little affected by further increase of the Cu content.

It should be noted that this reasoning does not apply to the $CaCuGe_2O_6$ compound as Cu occupies the M1 site (Redhammer *et al.*, 2004). The M2 site occupied by larger 7-coordinate Ca^{2+} cations (ionic radius 1.06 Å) now displays a quite small distortion and a larger average distance of 2.474(1) Å. Clearly, due to its large ionic radius, Ca^{2+} can only be accommodated at the M2 site and Cu^{2+} has to go to M1. The M1–O average bond length is 2.116(1) Å. Additional distortion could result from the JT effect induced by the Cu^{2+} cations.

Following our analysis of clinopyroxene silicates, it would tempting to propose that the driving force for the symmetry lowering between Cu-OP and Cu-CP can be the larger distortion brought about by the highest content of the JT Cu^{2+} cation at the M2 site. At first glance, this is supported by the fact that the Cr-CP compound containing 0.61 Cr^{2+} JT cations on the M2 site adopts the low-clinopyroxene structure with the $P2_1/c$ space group. However, one can see in Table 4 that the M2 site distortion for Cr-CP is much smaller than for Cu-OP, which could be related to the different *d*-orbital population of the Cr^{2+} and Cu^{2+} cations. Increasing distortion of the M2 site due to higher Cu^{2+} content may well be at the origin of symmetry lowering in Cu-bearing pyroxenes.

Conclusion

The structural investigation of the new $Cu_{0.8}Mg_{1.2}Si_2O_6$ clinopyroxene compound allows a comparative study of the effect of JT cation insertion in pyroxene compounds. It indicates that the marked preference of JT cations for the pyroxene M2 site is most probably related to its pre-existing distortion. Additional distortion brought about by the JT effect is controlled by the pyroxene topology and enhances the M2-site distortion. It is tempting to extend this assumption to other chain silicates and further investigations are required to check whether it can be turned into a general rule. For physicists, the tendency of divalent JT cations to occupy the M2 sites with very weak magnetic interactions make such systems unsuitable for displaying unusual magnetic properties. Our observations indicate that increasing the JT cation content leads to (and probably is the driving force for) symmetry lowering from ortho- to clinopyroxene. The extent to which such a strong site distortion can be accommodated by the pyroxene arrangement probably puts a limit on the maximum JT cation content even in the low-symmetry phase.

Acknowledgements

The authors are grateful to Dr Mehdi Mevel for discussions. This work was supported by a China Scholarship Council (CSC).

References

Angel, R.J, Gasparik, T. and Finger, L.W. (1989) Crystal structure of a Cr^{2+}-bearing pyroxene. *American Mineralogist*, **74**, 599–603.

Bérar, J-F. and Baldinozzi, G. (1993) Modeling of line-shape asymmetry in powder diffraction. *Journal of Applied Crystallography*, **26**, 128–129.

Breuer, K.H., Eysel, W. and Behruzi, M. (1986) Copper (II) silicates and germinates with chain structures. *Zeitschrift für Kristallographie*, **176**, 219–232.

Cameron, M. and Papike, J.J. (1981) Structural and chemical variations in pyroxenes. *American Mineralogist*, **66**, 1–50.

Favre-Nicolin, V. and Cerny, R. (2002) FOX, 'free objects for crystallography': a modular approach to *ab initio* structure determination from powder diffraction. *Journal of Applied Crystallography*, **35**, 734–743.

Finger, L.W., Hazen, R.M. and Hemley, R.J. (1989) $BaCuSi_2O_6$: a new cyclosilicate with four-membered tetrahedral rings. *American Mineralogist*, **74**, 952–955.

Isobe, M., Ninomiya, E., Vasilev, A.N. and Ueda, Y. (2002) Novel phase transition in spin-1/2 linear chain systems: $NaTiSi_2O_6$ and $LiTiSi_2O_6$. *Journal of the Physical Society of Japan*, **71**, 1423–1426.

Jodlauk, S., Becker, P., Mydosh, J.A., Khomskii, D.I., Lorenz, T., Streltsov, S.V., Hezel, D.C. and Bohaty, L. (2007) Pyroxenes: a new class of multiferroics. *Journal of Physics: Condensed Matter*, **19**, 432201–432209.

Kim, I., Jeon, G.G., Patil, D., Patil, S., Nenert, G. and Kin, K.H. (2012) Observation of multiferroic properties in pyroxene $NaFeGe_2O_6$. *Journal of Physics: Condensed Matter*, **24**, 306001–306007.

Makovicky, E. and Balic-Zunic, T. (1998) New measure of distortion for coordination polyhedra. *Acta Crystallographica*, **B54**, 766–773.

Nenert, G., Isobe, M., Kim, I., Ritter, C., Colin, C.V., Vasiliev, A.N., Kim, K.H. and Ueda, Y. (2010*a*) Interplay between low dimensionality and magnetic frustration in the magnetoelectric pyroxenes

https://doi.org/10.1180/minmag.2016.080.002 Published online by Cambridge University Press

$LiCrX_2O_6$ (X = Ge, Si). *Physical Review B*, **82**, 024429.

Nenert, G., Kim, I., Isobe, M., Ritter, C., Vasiliev, A.N., Kim, K.H. and Ueda, Y. (2010*b*) Magnetic and magnetoelectric study of the pyroxene $NaCrSi_2O_6$. *Physical Review B*, **81**, 184408.

Ohashi, Y. and Finger, L.W. (1976) The effect of Ca substitution on the structure of clinoenstatite. *Carnegie Institution of Washington Yearbook*, **75**, 743–746.

Redhammer, G.J. and Roth, G. (2004) Structural changes upon the temperature dependent $C2/c$-$P2_1/c$ phase transition in $LiMe^{3+}Si_2O_6$ clinopyroxenes, Me = Cr, Ga, Fe, V, Sc and In. *Zeitschrift für Kristallographie*, **219**, 585–605.

Redhammer, G.J., Tippelt, G., Merz, M., Roth, G., Treutmann, W. and Amthauer, G. (2005) Structure of the clinopyroxene-type compound $CaCuGe_2O_6$ between 15 and 800 K. *Acta Crystallographica*, **B61**, 367–380.

Redhammer, G.J., Roth, G., Treutmann, W., Hoelzel, M., Paulus, W., Andre, G., Pietzonka, C. and Amthauer, G. (2009) The magnetic structure of clinopyroxene-type $LiFeGe_2O_6$ and revised data on multiferroic $LiFeSi_2O_6$. *Journal of the Solid State Chemistry*, **182**, 2374–2384.

Redhammer, G.J., Senyshyn, A., Meven, M., Roth, G., Prinz, S., Pachler, A., Tippelt, G., Pietzonka, C., Treutmann, W., Hoelzel, M., Pedersen, B. and Amthauer, G. (2011) Nuclear and incommensurate magnetic structure of $NaFeGe_2O_6$ between 5 K and 298 K and new data on multiferroic $NaFeSi_2O_6$. *Physics and Chemistry of Minerals*, **38**, 139–157.

Redhammer, G.J., Roth, G., Senyshyn, A., Tippelt, G. and Pietzonka, C. (2013) Crystal and magnetic spin structure of germanium-hedenbergite, $CaFeGe_2O_6$, and a comparison with other magnetic/magnetoelectric/multiferroic pyroxenes. *Zeitschrift für Kristallographie*, **228**, 140–150.

Rodríguez-Carvajal, J. (1993) Recent advances in magnetic structure determination by neutron powder diffraction. *Physica B*, **192**, 55–69.

Rodríguez-Carvajal, J. (2010) *BondStr*. Available from www.ill.eu/sites/fullprof/

Sasago, Y., Hase, M. and Uchinokura, K. (1995) Discovery of a spin-singlet ground state with an energy gap in $CaCuGe_2O_6$. *Physical Review B*, **52**, 3533–3539.

Shannon, R.D. (1976) Revised effective ionic radii and systematic studies of interatomic distances in halides and chalcogenides. *Acta Crystallographica*, **A32**, 751–767.

Sparta, K.M. and Roth, G. (2004) Reinvestigation of the structure of $BaCuSi_2O_6$ – evidence for a phase transition at high temperature. *Acta Crystallographica*, **B60**, 491–495.

Tachi, T., Horiuchi, H. and Nagasawa, H. (1997) Structure of Cu-bearing orthopyroxene, $Mg(Cu_{.56},Mg_{.44})Si_2O_6$, and behavior of Cu^{2+} in the orthopyroxene structure. *Physics and Chemistry of Minerals*, **24**, 463–476.

Thompson, R.M. and Downs, R.T. (2003) Model pyroxenes I: ideal pyroxene topologies. *American Mineralogist*, **88**, 653–666.

Thompson, R.M. and Downs, R.T. (2004) Model pyroxenes II: structural variation as a function of tetrahedral rotation. *American Mineralogist*, **89**, 614–628.

Thompson, P., Cox, D.E. and Hastings, J.B. (1987) Rietveld refinement of Debye-Scherrer synchrotron X-ray data from Al_2O_3. *Journal of Applied Crystallography*, **20**, 79–83.

Thompson, R.M., Downs, R.T. and Redhammer, G.J. (2005) Model pyroxenes III: volume of $C2/c$ pyroxenes at mantle *P, T*, and *x*. *American Mineralogist*, **90**, 1840–1851.

Valenti, R., Saha, D.T. and Gros, C. (2002) Nature of the spin-singlet ground state in $CaCuGe_2O_6$. *Physical Review B*, **66**, 054426.

https://doi.org/10.1180/minmag.2016.080.002 Published online by Cambridge University Press